PHYSICAL REVIEW FLUIDS **1**, 082402(R) (2016)

Semiflexible particles in isotropic turbulence

Aamir Ali,[1,2] Emmanuel Lance Christopher VI Medillo Plan,[1]
Samriddhi Sankar Ray,[3] and Dario Vincenzi[1]
[1]*Université Côte d'Azur, CNRS, LJAD, 06108 Nice, France*
[2]*Department of Mathematics, COMSATS Intitute of Information Technology, Attock 43600, Pakistan*
[3]*International Center for Theoretical Sciences, Tata Institute of Fundamental Research, Bangalore 560089, India*

(Received 31 July 2016; published 9 December 2016)

The Lagrangian dynamics of semiflexible particles in homogeneous and isotropic turbulent flows is studied by means of analytically solvable stochastic models and direct numerical simulations. The stationary statistics of the bending angle shows a strong dependence on the dimension of the flow. In two-dimensional turbulence, particles are found in either a fully extended or a fully folded configuration; in three dimensions, the predominant configuration is the fully extended one. Such a sensitivity of the bending statistics on the dimensionality of the flow is peculiar to fluctuating flows and is not observed in laminar stretching flows.

DOI: 10.1103/PhysRevFluids.1.082402

The study of hydrodynamic turbulence and turbulent transport has received considerable impulse from the development of experimental, theoretical, and numerical Lagrangian techniques with applications to geophysics, astrophysics, and chemical engineering [1–4]. The translational dynamics of tracer and inertial pointlike particles is, for instance, intimately related to the mixing properties of turbulent flows [5]. In recent years, increasing attention has been drawn to the Lagrangian dynamics of microscopic objects that possess a complex shape or internal degrees of freedom, such as elastic dumbbells (see Ref. [6] and references therein), solid spheroids [7–11] and ellipsoids [12], bead-rod-spring chains [13], crosses and jacks [14], helicoids [15], and chiral dipoles [16].

We study the Lagrangian statistics of yet another internal degree of freedom, i.e., we examine the ability of a turbulent flow to bend a semiflexible particle. As a minimal model, we consider the trumbbell, which consists of three beads connected by two rigid rods and an elastic hinge at the middle [17]. The trumbbell model (also known as the trimer or three-bead two-rod model) was initially introduced in chemical physics to study solutions of stiff macromolecules [17–20]. It also represents the prototypical system for showing that the infinite-stiffness limit of elastic bonds is singular [21]. Here we regard the trumbbell as a simple model that allows us to isolate the bending dynamics of a semiflexible particle from the evolution of other potential degrees of freedom. This approach thus permits us to obtain the probability distribution of the bending angle analytically for laminar and random flows and numerically for fully developed turbulence. We show that the stationary statistics of the bending internal angle depends strongly on the dimension of the flow and on its turbulent character. In a two-dimensional (2D) homogeneous and isotropic incompressible turbulent flow, the distribution of the bending angle is bimodal; the configurations in which the trumbbell is either extended or folded are most probable, with the folded configuration being the most likely for strong turbulence. By contrast, in 3D turbulence, the extended configuration dominates and becomes increasingly probable as the amplitude of the velocity gradient increases. Such a sensitivity of the bending statistics on the flow dimensionality is peculiar to fluctuating flows and is not observed in laminar stretching flows.

A trumbbell consists of three identical beads joined by two inertialess rods of equal length ℓ immersed in a Newtonian fluid (Fig. 1) [17,18]. The drag force acting on the beads is given by the Stokes law with a drag coefficient ζ. An elastic hinge at the middle models the entropic forces that oppose the bending of the trumbbell; the force exerted by the hinge is described by a harmonic

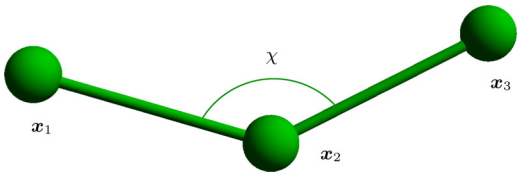

FIG. 1. Trumbbell model.

potential. The size of the trumbbell is sufficiently small for (a) it to experience Brownian fluctuations and (b) the velocity gradient $\nabla \boldsymbol{u}$ to be spatially uniform across the trumbbell. The inertia of the beads and the hydrodynamic interactions between them are disregarded [22,23]. Furthermore, the suspension is dilute; hence, particle-particle hydrodynamic interactions are negligible.

The positions of the beads are denoted by $\boldsymbol{x}_\nu$, $\nu = 1,2,3$. Under the above assumptions, the position of the center of mass $\boldsymbol{x}_c \equiv (\boldsymbol{x}_1 + \boldsymbol{x}_2 + \boldsymbol{x}_3)/3$ evolves like that of a tracer, i.e., $\dot{\boldsymbol{x}}_c(t) = \boldsymbol{u}(\boldsymbol{x}_c(t),t)$. The separation vectors between the beads and $\boldsymbol{x}_c$ are $\boldsymbol{r}_\nu \equiv \boldsymbol{x}_\nu - \boldsymbol{x}_c$. The configuration of the trumbbell in the reference frame of $\boldsymbol{x}_c$ is conveniently described in terms of $2(d-1)$ angular coordinates $\boldsymbol{q}$, where d is the dimension of the fluid [18]. For $d = 2$, $\boldsymbol{q} = (\theta,\chi)$, where $0 \leqslant \theta < 2\pi$ gives the orientation of $\boldsymbol{x}_3 - \boldsymbol{x}_2$ with respect to a fixed frame of reference and $0 \leqslant \chi < \pi$ is the internal angle between $\boldsymbol{x}_1 - \boldsymbol{x}_2$ and $\boldsymbol{x}_3 - \boldsymbol{x}_2$ (Fig. 1). By letting χ vary between 0 and π only, we do not distinguish between the two configurations that are obtained by exchanging $\boldsymbol{x}_1$ and $\boldsymbol{x}_3$. For $d = 3$, $\boldsymbol{q} = (\alpha,\beta,\gamma,\chi)$, where $0 \leqslant \chi < \pi$ is again the internal angle (Fig. 1) and $0 \leqslant \alpha < 2\pi$, $0 \leqslant \beta < \pi$, and $0 \leqslant \gamma < 2\pi$ are the Euler angles that specify the orientation of the orthogonal triad $(\boldsymbol{x}_3 - \boldsymbol{x}_1) \wedge (\boldsymbol{x}_2 - \boldsymbol{x}_c), \boldsymbol{x}_3 - \boldsymbol{x}_1, \boldsymbol{x}_2 - \boldsymbol{x}_c$ with respect to a fixed coordinate system. The relation between $\boldsymbol{r}_\nu$ and $\boldsymbol{q}$ is given in Ref. [24] for $d = 2$ and in Refs. [17,18] for $d = 3$.

The statistics of the configuration of the trumbbell is specified by the probability density function (PDF) $\Psi(\boldsymbol{q};t)$, which is such that $\int \Psi(\boldsymbol{q};t)d\boldsymbol{q} = 1$, and satisfies the following diffusion equation with periodic boundary conditions (summation over repeated indices is understood throughout this paper) [17,18]:

$$\partial_t \Psi = -\partial^i \left\{ \mathcal{G}^{ij} \left[\kappa^{kl}(t) r_\nu^l \left(\partial^j r_\nu^k\right) \Psi - \zeta^{-1} (\partial^j \phi) \Psi - KT\zeta^{-1} \sqrt{h} \partial^j (\Psi/\sqrt{h}) \right] \right\}, \tag{1}$$

where $\partial^i \equiv \partial/\partial q^i$, $\kappa^{ij}(t) = \partial^j u^i(t)$ is the velocity gradient evaluated at $\boldsymbol{x}_c(t)$, ζ is the drag coefficient of the beads, K is the Boltzmann constant, T is temperature, $\phi = \mu(\chi - \chi_\star)^2/2$ with $\chi_\star = \pi$ is the restoring potential, $\mathcal{G} = \mathcal{H}^{-1}$ with $\mathcal{H}^{ij} = \frac{\partial r_\nu^k}{\partial q^i} \frac{\partial r_\nu^k}{\partial q^j}$, and $h = \det(\mathcal{H})$. The explicit expressions of h and $\mathcal{G}$ can be found in Ref. [24] for $d = 2$ and in Ref. [18] for $d = 3$. Note that the stationary PDF of $\boldsymbol{q}$, $\Psi_{\rm st}(\boldsymbol{q})$, takes the form $\Psi_{\rm st}(\boldsymbol{q}) = J\psi_{\rm st}(\boldsymbol{q})$, where J is proportional to the Jacobian of the transformation from the $\boldsymbol{r}_\nu$ to the $\boldsymbol{q}$ coordinates; $J = 1$ for $d = 2$ and $J = \sin\chi \sin\beta$ for $d = 3$.

In the absence of flow gradients ($\boldsymbol{\kappa} = 0$) and the restoring potential ($\mu = 0$), $\Psi_{\rm st}(\boldsymbol{q}) = J\psi_0(\chi)$ with $\psi_0(\chi) \propto \sqrt{4 - \cos^2\chi}$ [17]. Thus, the configuration with the rods being perpendicular ($\chi = \pi/2$) has slightly greater probability than the other configurations, while the folded ($\chi = 0$) and the extended ($\chi = \pi$) configurations are equally probable. The restoring potential breaks this symmetry. For $\mu \neq 0$, $\psi_{\rm st}(\chi) \propto \psi_0(\chi)\exp[-Z(\chi_\star - \chi)^2/2]$ [17], where $Z \equiv \mu/KT$ is a stiffness parameter; the extended configuration is the most probable one and its probability increases as Z increases. Finally, when the trumbbell is introduced in a nonuniform flow ($\boldsymbol{\kappa} \neq 0$) its dynamics results from the interplay between the restoring elastic force and the deformation by the flow.

We first examine the effect of pure stretching on the statistics of the bending angle χ. Consider a 2D extensional flow $\boldsymbol{u} = \sigma(x,-y)$. As $\boldsymbol{\kappa} = \boldsymbol{\kappa}^\top$, the stationary solution of Eq. (1) is known analytically: $\Psi_{\rm st}(\theta,\chi) \propto \sqrt{h}\exp[(\Phi - \phi)/KT]$ with $\Phi = (\zeta/2)\kappa^{ij} r_\nu^i r_\nu^j$ [17]. The statistics of χ varies according to the orientation θ of the trumbbell; however, the average effect of the flow can be understood by considering the marginal stationary PDF of χ: $\hat{\Psi}_{\rm st}(\chi) = J\hat{\psi}_{\rm st}(\chi)$ with $\hat{\psi}_{\rm st}(\chi) \propto \psi_0(\chi)\exp[-Z(\chi_\star - \chi)^2/2] I_0[Z(1 - 2\cos\chi){\rm Wi}/3]$, where I_0 is the modified Bessel function of the first kind of order 0

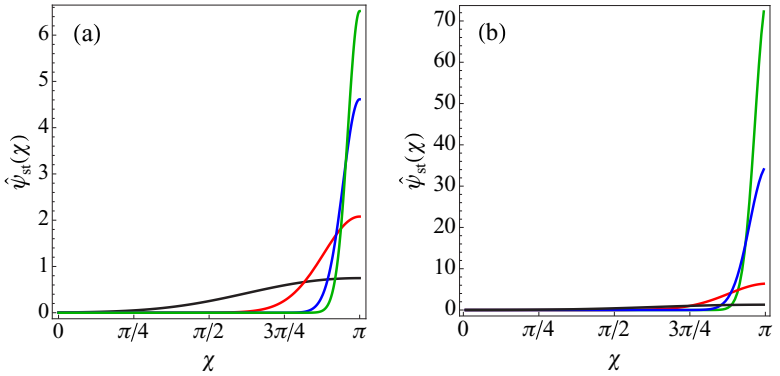

FIG. 2. Extensional flow: $\hat{\psi}_{st}(\chi)$ for (a) $d = 2$ and (b) $d = 3$, $Z = 1$, and $\mathrm{Wi} = 0$ (black line), $\mathrm{Wi} = 10$ (red line), $\mathrm{Wi} = 50$ (blue line), and $\mathrm{Wi} = 100$ (green line).

and the Weissenberg number $\mathrm{Wi} = \sigma\tau$ measures the relative strength of the flow and the restoring potential ($\tau = \zeta\ell^2/\mu$ is the characteristic time scale of the restoring potential). The product of Z and Wi yields the Péclet number $\mathrm{Pe} = \sigma\ell^2\zeta/KT$. On average, the 2D extensional flow favors the $\chi = \pi$ configuration, with this effect becoming stronger as Wi increases [Fig. 2(a)]. A linear stability analysis indeed shows that, when the flow dominates over the restoring potential ($\mathrm{Wi} \gg 1$) and thermal noise is disregarded, both the folded and the extended configurations are stable and their stability improves with increasing Wi, but the latter configuration is more attractive than the former for all Wi [24]. For a 3D uniaxial extensional flow $\boldsymbol{u} = \sigma(x, -y/2, -z/2)$, $\hat{\psi}_{st}(\chi)$ can again be calculated by using $\boldsymbol{\kappa} = \boldsymbol{\kappa}^\top$ and is shown in Fig. 2(b). Clearly, $\hat{\psi}_{st}(\chi)$ has a similar shape in two and three dimensions. Nevertheless, an inspection of the temporal dynamics of the trumbbell reveals a strong dependence on the dimension of the flow. To illustrate this point, we consider the situation in which the flow dominates over the restoring force ($\mathrm{Wi} \gg 1$ and $Z = 0$) and study the temporal evolution of $\chi(t)$ as a function of Pe. In particular, it is useful to analyze the average time T_0 it takes for an initially folded trumbbell to exit the interval $(0, \Delta\chi)$; T_0 is shown in Fig. 3 as a function of $\Delta\chi$ and Pe. The exit time T_0 behaves similarly for $d = 2$ and for $d = 3$. For small values of $\Delta\chi$, $T_0 \propto (\Delta\chi)^2$ because the dynamics is dominated by thermal noise, it keeps increasing as a function of $\Delta\chi$ until $\Delta\chi \approx \pi/2$, and it then becomes independent of $\Delta\chi$ because the average time

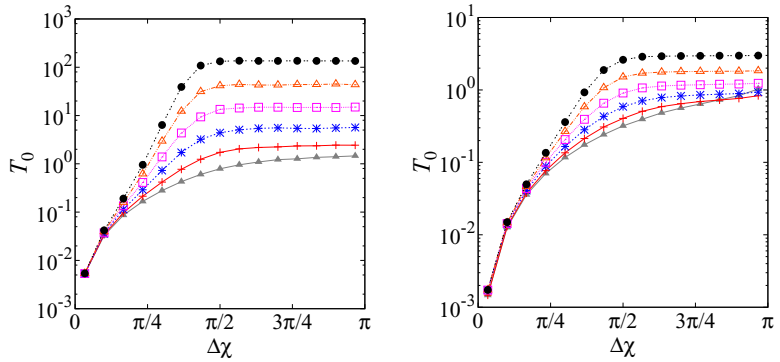

FIG. 3. Extensional flow: T_0 vs $\Delta\chi$ for (a) $d = 2$, $Z = 0$, and (from bottom to top) $\mathrm{Pe} = 4, 8, 12, 16, 20, 24$ and (b) $d = 3$ and the same values of Z and Pe as in (a). Here T_0 is calculated through a Monte Carlo simulation of the stochastic differential equations that govern the Lagrangian dynamics of the trumbbell for $d = 2$ and 3 (see Ref. [24]).

required to completely unfold a trumbbell with $\chi > \pi/2$ is much shorter than the time it takes to unfold an initially folded trumbbell up to $\chi \approx \pi/2$. However, for comparable values of Pe, T_0 is at least one order of magnitude longer in two dimensions than in three. The reason for this difference is geometrical: For $d = 2$ there are two degrees of freedom of the trumbbell, whereas there are four for $d = 3$; hence in the latter case it is easier for thermal noise to move the system away from the folded configuration. Such dependence of the dynamics on the spatial dimension d does not affect the shape of $\hat{\psi}_{\rm st}(\chi)$, because $\boldsymbol{\kappa}$ is constant and the system has the time to evolve to its stationary configuration. However, the flow dimension may impact the stationary statistics of χ in a turbulent flow, since in such a flow $\boldsymbol{\kappa}$ fluctuates.

In order to investigate this point analytically, we consider the Kraichnan random flow [25] in the Batchelor regime. The velocity gradient is a δ-correlated-in-time $(d \times d)$-dimensional Gaussian stochastic process with zero mean and correlation: $\langle \kappa^{ij}(t)\kappa^{kl}(t')\rangle = \mathcal{K}^{ijkl}\delta(t-t')$, where $\mathcal{K}^{ijkl} = 2\lambda[(d+1)\delta^{ik}\delta^{jl} - \delta^{ij}\delta^{kl} - \delta^{il}\delta^{jk}]/d(d-1)$ and λ is the Lyapunov exponent of the flow. The form of the tensor $\mathcal{K}$ ensures that the flow is incompressible and statistically isotropic. Although the assumption of temporal decorrelation is unrealistic, the study of this flow has contributed substantially to the understanding of turbulent transport, because it allows an analytical approach to this problem [1]. Let $P(\boldsymbol{q};t)$ be the PDF of the configuration of the trumbbell with respect to the realizations both of $\boldsymbol{\kappa}(t)$ and of thermal noise [$\int P(\boldsymbol{q};t)d\boldsymbol{q} = 1$]; $P(\boldsymbol{q};t)$ solves the diffusion equation [13]

$$\partial_t P = \partial^i \left\{ \tfrac{1}{2}\mathcal{K}^{klmn}\mathcal{G}^{ij} r_\nu^l \left(\partial^j r_\nu^k\right)\partial^a \left[\mathcal{G}^{ab} r_\rho^n \left(\partial^b r_\rho^m\right) P\right] + \mathcal{G}^{ij}\zeta^{-1}[(\partial^j\phi)P + KT\sqrt{h}\partial^j(P/\sqrt{h})]\right\}. \quad (2)$$

Let us first consider the 2D case. By using $\boldsymbol{q} = (\theta, \chi)$ and the corresponding $\mathcal{G}$, we can rewrite Eq. (2) as a Fokker-Planck equation (FPE) in the variables θ and χ. The drift and diffusion coefficients, however, do not depend on θ because of statistical isotropy. Hence the stationary PDF of the configuration is a function of χ alone and is the stationary solution of the following FPE in one variable:

$$\partial_s P = -\partial_\chi(VP) + \tfrac{1}{2}\partial^2_{\chi\chi}(DP), \quad (3)$$

with $s = t/\tau$,

$$V(\chi) = \frac{12\sin\chi}{Z(2-\cos\chi)(2+\cos\chi)^2} + \frac{6(\chi_\star - \chi)}{(2+\cos\chi)} + 2\,\mathrm{Wi}\frac{\sin\chi[5+\cos\chi - 11\cos(2\chi) - \cos(3\chi)]}{(2-\cos\chi)(2+\cos\chi)^3}, \quad (4)$$

and $D(\chi) = 12/Z(2+\cos\chi) + 16\,\mathrm{Wi}\sin^2\chi/(2+\cos\chi)^2$, where now $\mathrm{Wi} = \lambda\tau$. The stationary solution of Eq. (3) that satisfies periodic boundary conditions is [26]

$$P_{\rm st}(\boldsymbol{q}) = J p_{\rm st}(\chi) \propto \exp\left[2\int_0^\chi d\eta\, V(\eta)/D(\eta)\right] \Big/ D(\chi). \quad (5)$$

The function $p_{\rm st}(\chi)$ is plotted in Fig. 4(a) for different values of Wi. For small Wi, the most probable configuration is the $\chi = \pi$ one, as in the hyperbolic flow. However, as Wi increases, a second peak emerges near $\chi = 0$, while intermediate values of χ become less and less probable. At large Wi, $p_{\rm st}(\chi)$ consists of two narrow peaks, one at $\chi = \pi$ and the other approaching $\chi = 0$, with the latter becoming more and more pronounced with increasing Wi.

In three dimensions, Eq. (2) can be rewritten as a FPE in the variables $\alpha, \beta, \gamma, \chi$. Owing to statistical isotropy, $P_{\rm st}(\boldsymbol{q})$ is again the stationary solution of a FPE in the variable χ alone and takes

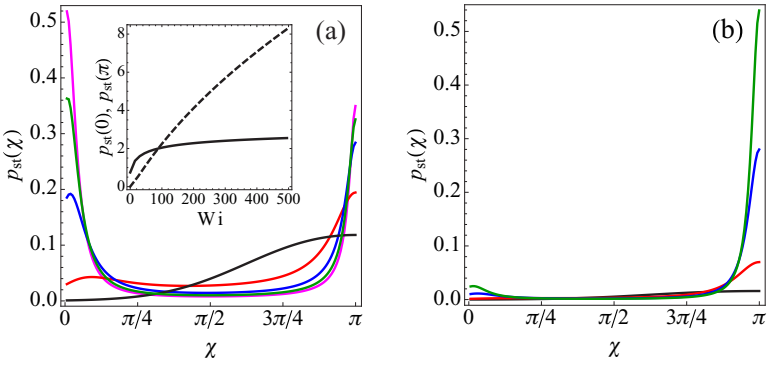

FIG. 4. Batchelor-Kraichnan flow: (a) $p_{st}(\chi)$ for $d = 2$, $Z = 1$, and $\mathrm{Wi} = 0$ (black line), $\mathrm{Wi} = 10$ (red line), $\mathrm{Wi} = 50$ (blue line), $\mathrm{Wi} = 100$ (green line), and $\mathrm{Wi} = 150$ (magenta line). The inset shows the values of $p_{st}(\chi)$ at $\chi = 0$ (dashed line) and $\chi = \pi$ (solid line) vs Wi. (b) $p_{st}(\chi)$ for $d = 3$ and the same values of Z and Wi as in (a).

the form in Eq. (5) with

$$V(\chi) = \frac{3[4 + 13\cos\chi - 4\cos(2\chi) - \cos(3\chi)]}{2Z\sin\chi(2 - \cos\chi)(2 + \cos\chi)^2} + \frac{6(\chi_\star - \chi)}{(2 + \cos\chi)} + \mathrm{Wi}\frac{\sin\chi[63\cos\chi - 15\cos(3\chi) + 296\sin^2\chi]}{12(2 - \cos\chi)(2 + \cos\chi)^3} \tag{6}$$

and $D(\chi) = 12/Z(2 + \cos\chi) + 26\,\mathrm{Wi}\sin^2\chi/3(2 + \cos\chi)^2$. Figure 4(b) shows that a tiny peak at $\chi = 0$ emerges only for very large Wi and the $\chi = \pi$ configuration prevails for all Wi. Thus, the statistics of χ is different in two and three dimensions. In particular, for $d = 3$, the behavior of $p_{st}(\chi)$ is similar to that found for the extensional flow.

The difference in the stationary statistics of χ for $d = 2$ and 3 can again be understood by assuming $\mathrm{Wi} = \infty$ and $Z = 0$ and by considering T_0 and the average time T_π it takes for an initially extended trumbbell ($\chi = \pi$) to exit the interval $(\pi - \Delta\chi, \pi)$ through the left. The ratio T_0/T_π is plotted in Fig. 5 vs $\Delta\chi$ for increasing Pe. For small $\Delta\chi$, $T_0 > T_\pi$ for both $d = 2$ and $d = 3$, because in the folded configuration the end beads have very similar velocities and is therefore difficult for the flow to separate them. However, T_0/T_π is greater for $d = 2$ than for $d = 3$; moreover, it grows fast as a function of Pe for $d = 2$ and is almost independent of Pe for $d = 3$. This is because for $d = 2$ the beads are confined to the plane and is much more difficult for the flow to separate them compared to the 3D case. When $\Delta\chi \approx \pi$, T_0 and T_π are comparable for $d = 2$, whereas $T_0 \ll T_\pi$ for $d = 3$, i.e., in this case the average time required to completely unfold an initially folded trumbbell is much shorter than that required to fold an initially extended one. The reason for this is once again geometrical; it is indeed more difficult to fold two rods whose orientations fluctuate in 3D space than to fold two rods that are confined to the plane. The above discussion explains why, for $d = 2$, $p_{st}(\chi)$ shows a second peak near $\chi = 0$ and this peak dominates for a strong flow, whereas $p_{st}(\chi)$ does not enjoy the same property for $d = 3$.

Are the results obtained so far valid in turbulent flows? To ensure that the qualitative properties of the statistics of χ do not depend on the Gaussianity and temporal decorrelation of the Batchelor-Kraichnan flow, we perform Lagrangian direct numerical simulations of the trumbbell model in 2D and 3D incompressible isotropic turbulence by using a standard pseudospectral method on a 2π-periodic domain. For $d = 2$, our simulation is forced at large scales and uses an air-drag-induced Ekman friction; the choice of the parameters [27,28] yields a Taylor-microscale Reynolds number $\mathrm{Re}_\lambda = 827$, in the nonequilibrium statistically steady state. For $d = 3$, the forcing has a fixed energy input [29,30] and $\mathrm{Re}_\lambda = 121$. We have done other simulations with different Re_λ and forcing scales

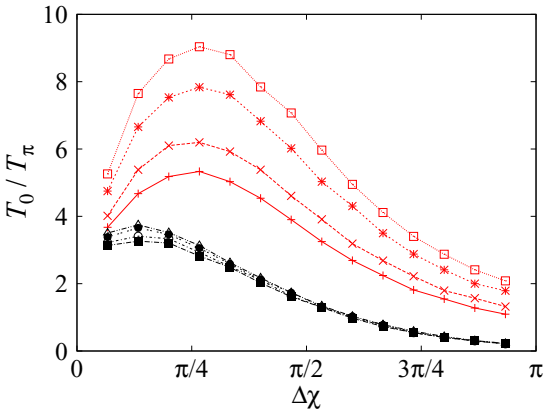

FIG. 5. Batchelor-Kraichnan flow: T_0/T_π vs $\Delta\chi$ for $d = 2$ (red) and $d = 3$ (black), $Z = 0$, and (from bottom to top) Pe $= 30,50,100,150$. Here T_0 and T_π are calculated from a numerical simulation of the Itô stochastic differential equation $\dot{\chi} = V(\chi) + \sqrt{D(\chi)}\,\xi(t)$ for $d = 2$ and of the analogous stochastic differential equation for $\cos\chi$ for $d = 3$ [here $\xi(t)$ is white noise].

that yield results consistent with the ones presented here. The flow is seeded with 10^5 trumbbells in two dimensions and with 10^6 trumbbells in three dimensions, each of whose center of mass evolves as a tracer; the velocity at $\boldsymbol{x}_c$ is evaluated from the Eulerian velocity by using a bilinear-interpolation scheme [27,28]. The statistics of χ is computed from a Lagrangian simulation of the stochastic differential equations for the configuration of the trumbbell [24]. The Weissenberg number is defined as for the random flow, i.e., Wi $= \lambda\tau$. The numerical results shown in Fig. 6 confirm the predictions based on the Batchelor-Kraichnan flow. In particular, for $d = 2$, the $\chi = \pi$ configuration is favored at small Wi. As Wi increases, the probability of a folded configuration grows significantly and eventually, at extremely large Wi, $p_{\rm st}(\chi)$ displays strong peaks at $\chi \approx 0$ and $\chi \approx \pi$, with the former peak prevailing over the latter. For $d = 3$, $p_{\rm st}(\chi)$ has a maximum at $\chi = \pi$, which grows with increasing Wi; a very small peak near $\chi = 0$ only appears for very large Wi.

We have studied the bending statistics of semiflexible particles in laminar and turbulent flows. By using analytical calculations and numerical simulations, we have shown that the stationary distribution of the bending internal angle depends strongly on whether the flow is laminar or

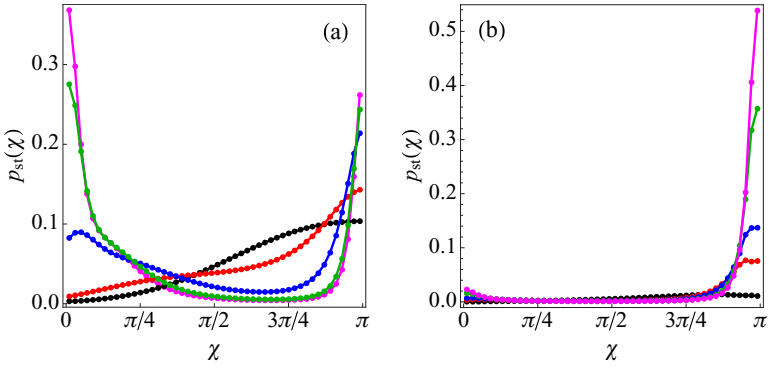

FIG. 6. Homogeneous isotropic turbulence: (a) $p_{\rm st}(\chi)$ for $d = 2$, $Z = 1$, and Wi $= 0.04$ (black line), Wi $=$ 17.53 (red line), Wi $= 45.3$ (blue line), Wi $= 54$ (green line), and Wi $= 102$ (magenta line) and (b) $p_{\rm st}(\chi)$ for $d = 3$, $Z = 1$, and Wi $= 3.3$ (black line), Wi $= 26.3$ (red line), Wi $= 49.3$ (blue line), Wi $= 131.4$ (green line), and Wi $= 197.1$ (magenta line).

turbulent and, in the turbulent case, is sensitive to the flow dimensionality. We have interpreted this behavior in terms of the mean exit times from the folded and the extended configurations. These results suggest that the rheology of suspensions of semiflexible particles may also exhibit an analogous strong dependence on the properties of the flow. We hope our work will lead to further experiments directed towards the study of the Lagrangian dynamics of semiflexible particles in turbulent flows and the non-Newtonian properties of turbulent suspensions of such particles.

The work of A.A. and E.L.C.M.P. was supported by EACEA through the Erasmus Mundus Mobility with Asia program. E.L.C.M.P., S.S.R., and D.V. acknowledge the support of the EU COST Action MP1305 "Flowing Matter". S.S.R. and D.V. thank the Indo-French Center for Applied Mathematics for financial support. S.S.R. acknowledges support from the AIRBUS Group Corporate Foundation Chair in Mathematics of Complex Systems established in ICTS-TIFR, the DST (India) Project No. ECR/2015/000361. D.V. would like to thank ICTS-TIFR for the kind hospitality. The direct numerical simulations were done on *Mowgli* at the ICTS-TIFR, Bangalore, India.

[1] G. Falkovich, K. Gawędzki, and M. Vergassola, Particles and fields in fluid turbulence, Rev. Mod. Phys. **73**, 913 (2001).

[2] R. Pandit, P. Perlekar, and S. S. Ray, Statistical properties of turbulence: An overview, Pramana **73**, 157 (2009).

[3] F. Toschi and E. Bodenschatz, Lagrangian properties of particles in turbulence, Annu. Rev. Fluid Mech. **41**, 375 (2009).

[4] J. P. L. C. Salazar and L. R. Collins, Two-particle dispersion in isotropic turbulent flows, Annu. Rev. Fluid Mech. **41**, 405 (2009).

[5] J. Bec, L. Biferale, G. Boffetta, M. Cencini, S. Musacchio, and F. Toschi, Lyapunov exponents of heavy particles in turbulence, Phys. Fluids **18**, 091702 (2006).

[6] S. Musacchio and D. Vincenzi, Deformation of a flexible polymer in a random flow with long correlation time, J. Fluid Mech. **670**, 326 (2011).

[7] A. Pumir and M. Wilkinson, Orientation statistics of small particles in turbulence, New J. Phys. **13**, 093030 (2011).

[8] S. Parsa, E. Calzavarini, F. Toschi, and G. A. Voth, Rotation Rate of Rods in Turbulent Fluid Flow, Phys. Rev. Lett. **109**, 134501 (2012).

[9] D. Vincenzi, Orientation of non-spherical particles in an axisymmetric random flow, J. Fluid Mech. **719**, 465 (2013).

[10] K. Gustavsson, J. Einarsson, and B. Mehlig, Tumbling of Small Axisymmetric Particles in Random and Turbulent Flows, Phys. Rev. Lett. **112**, 014501 (2014).

[11] A. Gupta, D. Vincenzi, and R. Pandit, Elliptical tracers in two-dimensional, homogeneous, isotropic fluid turbulence: The statistics of alignment, rotation, and nematic order, Phys. Rev. E **89**, 021001(R) (2014).

[12] L. Chevillard and C. Meneveau, Orientation dynamics of small, triaxial-ellipsoidal particles in isotropic turbulence, J. Fluid Mech. **737**, 571 (2013).

[13] E. L. C. VI M. Plan, A. Ali, and D. Vincenzi, Bead-rod-spring models in random flows, Phys. Rev. E **94**, 020501(R) (2016).

[14] G. G. Marcus, S. Parsa, S. Kramel, R. Ni, and G. A. Voth, Measurements of the solid-body rotation of anisotropic particles in 3D turbulence, New J. Phys. **16**, 102001 (2014).

[15] K. Gustavsson and L. Biferale, Preferential sampling of helicity by isotropic helicoids, Phys. Rev. Fluids **1**, 054201 (2016).

[16] S. Kramel, G. A. Voth, S. Tympel, and F. Toschi, Preferential Rotation of Chiral Dipoles in Isotropic Turbulence, Phys. Rev. Lett. **117**, 154501 (2016).

[17] O. Hassager, Kinetic theory and rheology of bead-rod models for macromolecular solutions. I. Equilibrium and steady flow properties, J. Chem. Phys. **60**, 2111 (1974); Kinetic theory and rheology of bead-rod models for macromolecular solutions. II. Linear unsteady flow properties, *ibid.* **60**, 4001 (1974).

[18] R. B. Bird, O. Hassager, R. C. Armstrong, and C. F. C. Curtiss, *Dynamics of Polymeric Liquids* (Wiley, New York, 1977), Vol. 2.

[19] D. B. Roitman, The elastic trumbbell model for dynamics of stiff chains, in *Rotational Dynamics of Small and Macromolecules*, Proceedings of a Workshop held at the Zentrum für interdisziplinäre Forschung Universität Bielefeld, Bielefield, edited by Th. Dormfüller and R. Pecora, Lecture Notes in Physics Vol. 293 (Springer, Berlin Heidelberg, 1987), p. 192.

[20] J. Garcia de la Torre, Hydrodynamics of segmentally flexible macromolecules, Eur. Biophys. J. **23**, 307 (1994).

[21] E. J. Hinch, Brownian motion with stiff bonds and rigid constraints, J. Fluid Mech. **271**, 219 (1994).

[22] F. G. Diaz and J. Garcia de la Torre, Simulation of the rotational Brownian dynamics of a simple, segmentally flexible model: The elastic trumbbell, J. Chem. Phys. **88**, 7698 (1988).

[23] R. J. Lewis, S. A. Allison, D. Eden, and R. Pecora, Brownian dynamics simulations of a three-subunit and a ten-subunit worm-like chain: Comparison of results with trumbell theory and with experimental results from DNA, J. Chem. Phys. **89**, 2490 (1988).

[24] E. L. C. VI M. Plan and D. Vincenzi, Tumbling of a Brownian particle in an extensional flow, Proc. R. Soc. London A **472**, 20160226 (2016).

[25] R. H. Kraichnan, Small-scale structure of a scalar field convected by turbulence, Phys. Fluids **11**, 945 (1968).

[26] H. Risken, *The Fokker-Planck Equation* (Springer, Berlin, 1989).

[27] P. Perlekar, S. S. Ray, D. Mitra, and R. Pandit, Persistence Problem in Two-Dimensional Fluid Turbulence, Phys. Rev. Lett. **106**, 054501 (2011).

[28] S. S. Ray, D. Mitra, P. Perlekar, and R. Pandit, Dynamic Multiscaling in Two-Dimensional Fluid Turbulence, Phy. Rev. Lett. **107**, 184503 (2011).

[29] A. G. Lamorgese, D. A. Caughey, and S. B. Pope, Direct numerical simulation of homogeneous turbulence with hyperviscosity, Phys. Fluids **17**, 015106 (2005).

[30] G. Sahoo, P. Perlekar, and R. Pandit, Systematics of the magnetic-Prandtl-number dependence of homogeneous, isotropic magnetohydrodynamic turbulence, New J. Phys. **13**, 013036 (2011).